Eur. Phys. J. Appl. Phys. (2012) 58: 30403
DOI: 10.1051/epjap/2012120157

THE EUROPEAN PHYSICAL JOURNAL APPLIED PHYSICS

Regular Article

Fabrication of graphene/polypyrrole nanotube/MnO_2 nanotube composite and its supercapacitor application

J. An[1], J. Liu[1,a], Y. Ma[1], R. Li[2], M. Li[1], M. Yu[1], and S. Li[1]

[1] School of Materials Science and Engineering, Beihang University, Beijing 100191, P.R. China
[2] Jiangsu Electric Power Maintenance Branch Company, State Grid Corporation of China (SGCC), Nanjing 211102, Jiangsu, P.R. China

Received: 25 April 2012 / Received in final form: 2 June 2012 / Accepted: 5 June 2012
Published online: 5 July 2012 –

Abstract. A novel composite is fabricated through hybridizing graphene with polypyrrole (PPY) nanotube and manganese dioxide (MnO_2) nanotube to comprehensively utilize the electrical double layer capacitance and pseudo-capacitance. Scanning electron microscopy (SEM), transmission electron microscopy (TEM) and Raman spectroscopy are employed to characterize its structure. The SEM and TEM images illustrate that graphene/PPY nanotube/MnO_2 nanotube composite (GPM) presents interconnected structure. The result of Raman analysis demonstrates the intimate interactions among PPY, graphene and MnO_2. In addition, cyclic voltammetry (CV), galvanostatic charge-discharge and electrochemical impedance spectroscopy (EIS) techniques are used to measure the electrochemical properties. It is revealed that GPM presents excellent high-rate performance and its capacitance is as high as 469.5 Fg^{-1} at a current density of 0.3 Ag^{-1}, higher than that of PPY and chemically reduced graphene sheet as well as the materials reported in the literature. Furthermore, long-term charge-discharge cycle test confirms that the fabrication of GPM can effectively merge the merits of graphene, PPY and MnO_2. Additionally, EIS analysis illustrates that the presence of conductive graphene as well as the intimate interactions among graphene, PPY and MnO_2 lead to the good electrochemical stability.

1 Introduction

On the wake of depletion of traditional energy resource, many attempts have been devoted to the development of renewable energy production [1]. As a promising energy storage device in a wide range of applications, the supercapacitor has attracted much attention in recent years [2–8]. Electrical double-layer (EDL) capacitor and pseudo-capacitor are two types of supercapacitors based on their difference in energy storage mechanisms. The EDL capacitor stores charge in the double layer of the electrode-electrolyte interface. Carbon-based materials that feature large specific area, such as active carbon [9], carbon nanotubes [10] and carbon aerogel [11,12], have been used in EDL supercapacitors. Lately, as a novel carbon material, graphene has generated widespread interest for its outstanding properties [13–21]. It has been used as energy storage material [22]. However, the capacitance values of these carbon-based materials are limited [23] (about 200 Fg^{-1}), although they usually display good electrochemical stability [24]. Pseudo-capacitor obtains capacitance from electrochemically active materials through rapid and reversible redox reaction. Conductive polymers such as polyaniline [25–27] and polypyrrole (PPY) [27–30] have been applied as pseudo-capacitor electrode materials and have shown high capacitance (about 400 Fg^{-1}) [27,31]. As a conductive polymer, however, PPY is limited in electrochemical stability because its structural conformation changes with repeated ion exchange in the electrochemical process, which consequently leads to the degradation of electrical properties [32]. Meanwhile, transition metal oxide such as manganese dioxide (MnO_2) [29,33] has also been conceived as promising pseudo-capacitor electrode material for its low cost and high specific capacitance (even up to 1380 Fg^{-1}) [34]. However, the electrical conductivity of MnO_2 is poor, and the pseudo-capacitive reaction of MnO_2 is surface reaction, in which only a very thin surface layer of the oxide can participate. The low conductivity and low accessible surface area of MnO_2 limit its application.

The graphene-PPY composites [35–44] and graphene-MnO_2 composites [34,45–50] have been proposed to comprehensively utilize the EDL capacitance and pseudo-capacitance, which significantly boost the materials' electrochemical performance. Inspired by the assembly of functionally gradient materials, the fabrication of highly conductive graphene with good conductivity PPY and poor conductivity MnO_2 may take the advantages of graphene and PPY as well as utilize the high capacitance

[a] e-mail: liujh@buaa.edu.cn

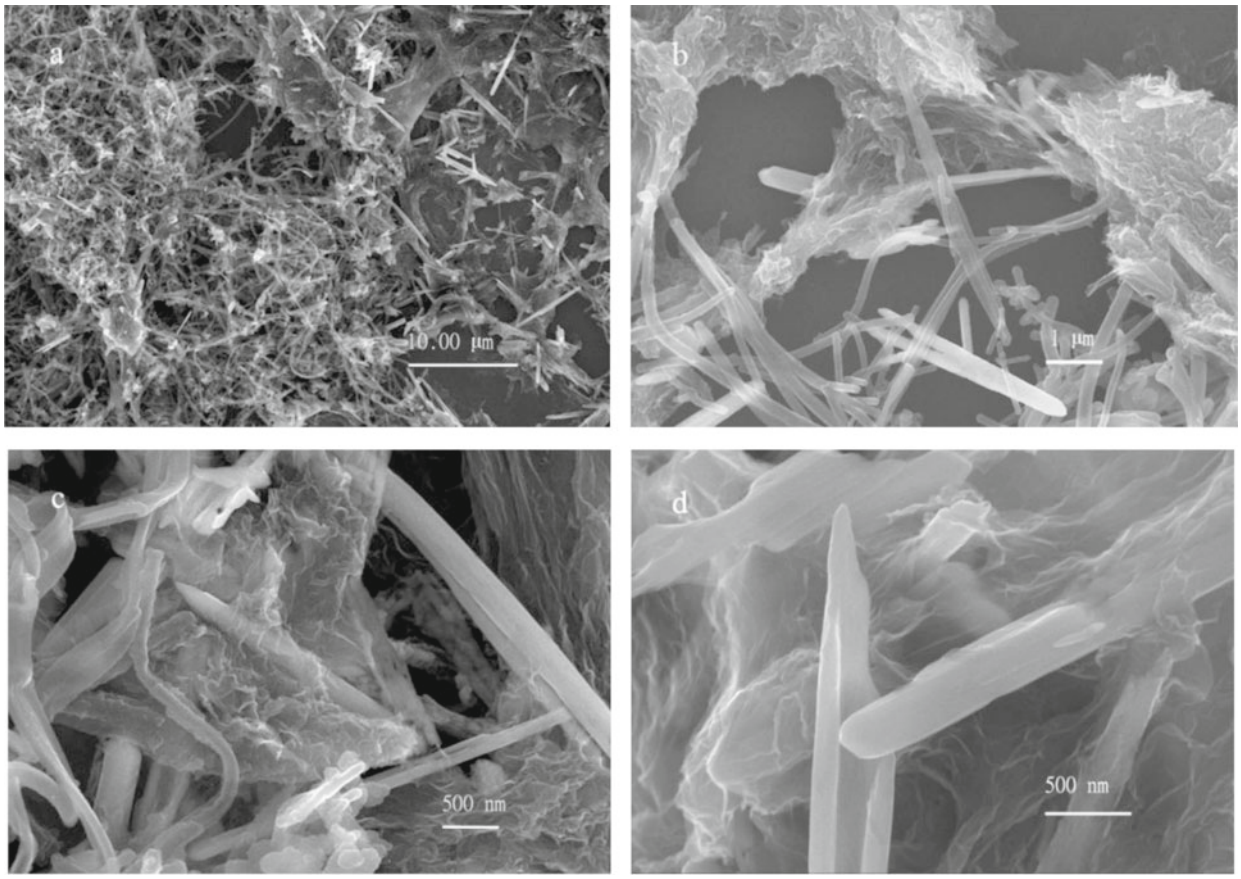

Fig. 1. SEM images of GPM: (a) overall morphology of GPM, (b) PPY nanotubes interspersing in graphene sheets, (c) coexistence of graphene, PPY and MnO_2 nanotubes and (d) graphene sheets wrapping MnO_2 nanotubes.

properties of PPY and MnO_2, and thus give a good performance. In this paper, graphene, PPY and MnO_2 were comprehensively utilized to incorporate the high stability of graphene with the high capacitance of PPY and MnO_2. As far as we know, the realization of high specific capacitance is only possible with effective electrolyte transport to the active sites for enhancing faradic charge-transfer reaction [35]. The nanotube structures of PPY and MnO_2 could enlarge the accessible pseudo-capacitive reaction area and consequently enhance the capacitance. Therefore, nanotube structures of PPY and MnO_2 were prepared, which are expected to show rapid ionic transport within the bulk matrix. Through mixing graphene with PPY nanotube and MnO_2 nanotube, the graphene/PPY nanotube/MnO_2 nanotube composite (GPM) was prepared. In order to study its potential application in supercapacitor, electrochemical performances were measured by using cyclic voltammetry (CV), galvanostatic charge-discharge and electrochemical impedance spectroscopy (EIS) techniques.

2 Experimental section

2.1 Preparation of graphene oxide

Graphene oxide was prepared in two steps: first, the oxidation of graphite followed a modified Hummers' method revealed in literature [51]. After oxidation, the obtained graphite oxide colloid was ultrasonicated to acquire graphene oxide colloid. Then, by diluting, centrifugation and drying, graphene oxide powder was obtained.

2.2 Preparation of chemically reduced graphene sheet (CRGS)

The preparation of CRGS followed a modified method reported by Tung et al. [52]. First, 1 g graphene oxide powder was dissolved in 250 mL N_2H_4 with ultrasonication for 15 min. Second, the solution was kept stirring for 24 h, and then the reactant mixture was kept still for one week. After the reaction, the resultant was centrifuged three times, then diluted and filtered through 0.22 μm porous PTFE membrane. The filtered cake was washed with 200 mL ethanol and 250 mL deionized water. Finally, after drying at 45 °C for 24 h, the CRGS was obtained.

2.3 Preparation of MnO_2 nanotube

The preparation of MnO_2 nanotube followed the processes reported by Shi et al. [53]. It is as follows: 0.02 mol $MnSO_4 \cdot H_2O$ was dissolved in 50 mL deionized water, and then 0.0225 mol polyvinyl pyrrolidone (polymerization degree: 360) was slowly added in with vigorously stirring.

https://doi.org/10.1051/epjap/2012120157 Published online by Cambridge University Press

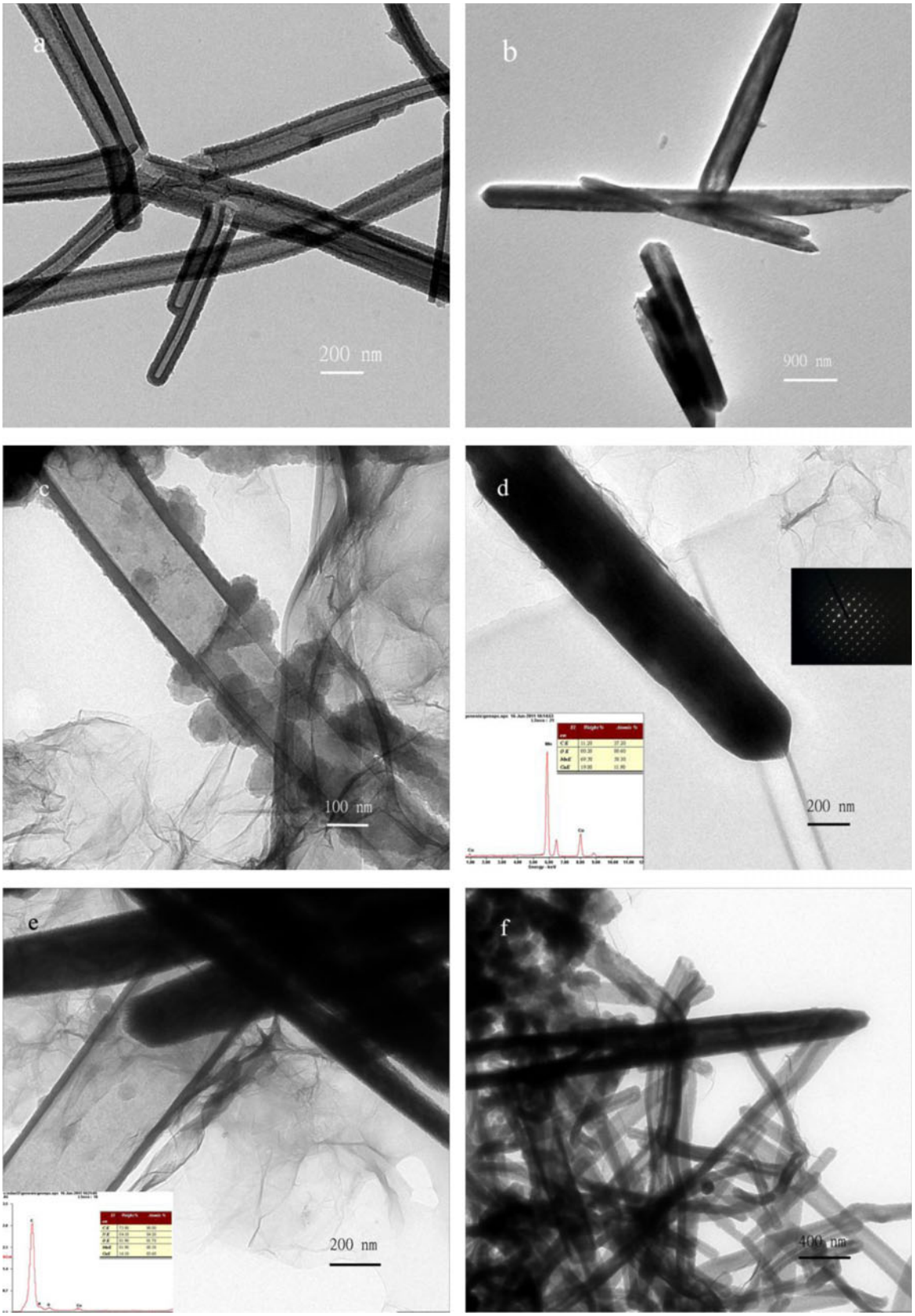

Fig. 2. (Color online) TEM images of PPY, MnO_2 and GPM: (a) PPY nanotubes, (b) MnO_2 nanotubes, (c) coexistence of graphene sheets and PPY nanotubes in GPM, (d) coexistence of graphene sheets and MnO_2 nanotubes in GPM, (e) and (f) interconnected structure of GPM.

https://doi.org/10.1051/epjap/2012120157 Published online by Cambridge University Press

When the solution became clear, 40 mL aqueous solution containing 0.04 mol $NaClO_3$ was added in with continuously stirring. The solution was transferred into a Teflon-lined stainless steel autoclave. The autoclave was sealed and maintained at 160 °C for 10 h. After the reaction completed, the product was filtered, washed and dried.

2.4 Preparation of PPY nanotube

The preparation of PPY nanotube followed a method reported by Yang et al. [54]. The typical processes are as follows: first, 0.784 g methyl orange and 3.888 g $FeCl_3$ were dissolved in 480 mL deionized water, and then 0.84 mL pyrrole was added in. The solution was kept stirring for 24 h. After stirring, the resultant was filtered and washed with deionized water. Then the product was dried at 40 °C for 8 h.

2.5 Preparation of GPM

First, 400 mg PPY nanotube was dissolved in a solution containing 5 mL dimethylformamide and 20 mL deionized water, and then kept ultrasonicating for 15 min. Second, 50 mg CRGS was dissolved in 100 mL deionized water with ultrasonication for 30 min. Third, 50 mg MnO_2 nanotube was added into the PPY solution and then it was poured into the CRGS solution with moderately stirring. The mixture was kept stirring for 24 h. After stirring, the product was filtered and washed.

2.6 Morpholgy and texture measurement

Transmission electron microscopy (TEM) measurement was conducted on a JEOL 2010 FEG microscope at 200 kV. Scanning electron microscopy (SEM) measurement was carried out on a JEOL-4800 microscope at 10 kV. Raman spectra were measured on a Horiba Jobin Yvon LabRAM HR 800 Raman spectrometer.

2.7 Electrochemical property measurements

The electrochemical measurements were measured in three-electrode test system, using platinum sheet as counter electrode, AgCl/Ag electrode as reference electrode and glassy-carbon electrode coated with sample as working electrode. The working electrode was prepared by casting a nafion-impregnated sample onto a glassy-carbon electrode with a diameter of 5 mm. Typically, 4 mg of composite was dispersed in 2 mL ethanol solution containing 5 μL of 5% nafion solution with ultrasonication for 5 min. This sample was dropped onto glassy-carbon electrode and dried at temperature. Galvanostatic charge-discharge, CV and EIS techniques were employed to evaluate the materials' electrochemical properties on a CHI potentiostation 660A at room temperature. The electrolyte is a 1M Na_2SO_4 aqueous solution. The specific capacitance (Cm) was calculated from the slope of the discharge curve, according to the equation $Cm = (I \times \Delta t)/(\Delta V \times m)$, where I is the constant discharge current, Δt is the discharge during time, ΔV is the voltage difference in discharge and m is the mass of the sample coated on working electrode.

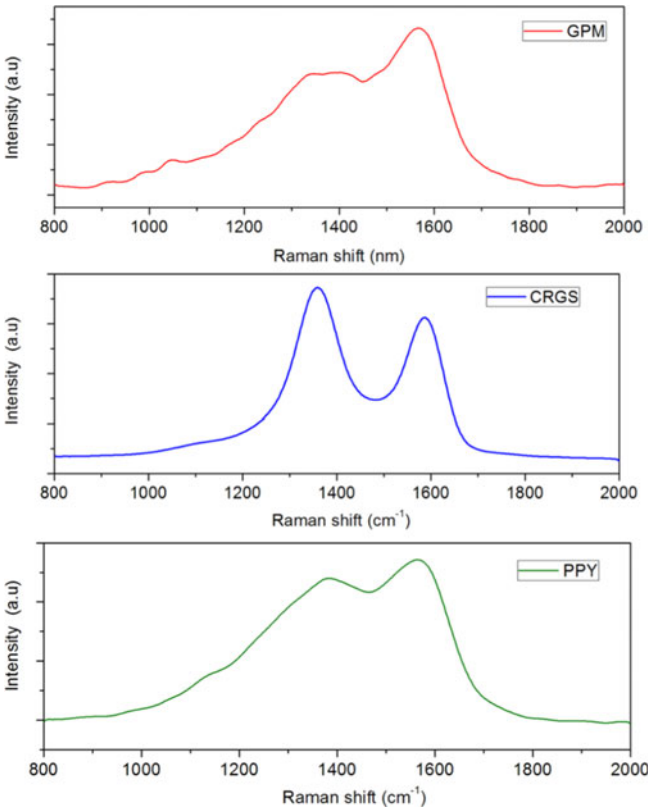

Fig. 3. (Color online) Raman spectra of GPM, CRGS and PPY.

3 Results and discussion

The SEM images in Figure 1 illustrate the morphology of GPM. As shown in Figure 1a, it is obvious that PPY nanotubes and MnO_2 nanotubes distribute well in GPM. Additionally, as presented in Figure 1b, PPY nanotubes twine graphene and MnO_2 nanotubes together to strengthen the material. Furthermore, as exhibited in Figures 1c and 1d, MnO_2 nanotubes are intimately wrapped by graphene sheets, and the diameter of MnO_2 nanotubes is 300 $\sim$ 500 nm, consistent with the result reported previously [53].

The TEM investigation further illustrates the intimate contact feature of GPM. In Figures 2a and 2b, the nanotube texture of PPY and MnO_2 can be observed. Figure 2c shows that PPY nanotube is enfolded by flexible graphene sheets. In Figure 2d, it exhibits that the ductile graphene sheets wrap the MnO_2 nanotube intimately. The obtained electron diffraction pattern of MnO_2 shows that it is in crystalline form, consistent with the result in literature [53]. In Figures 2e and 2f, a network structure of GPM is presented. The result of following EDS analysis in Figure 2d illustrates that the element Mn exists on the

https://doi.org/10.1051/epjap/2012120157 Published online by Cambridge University Press

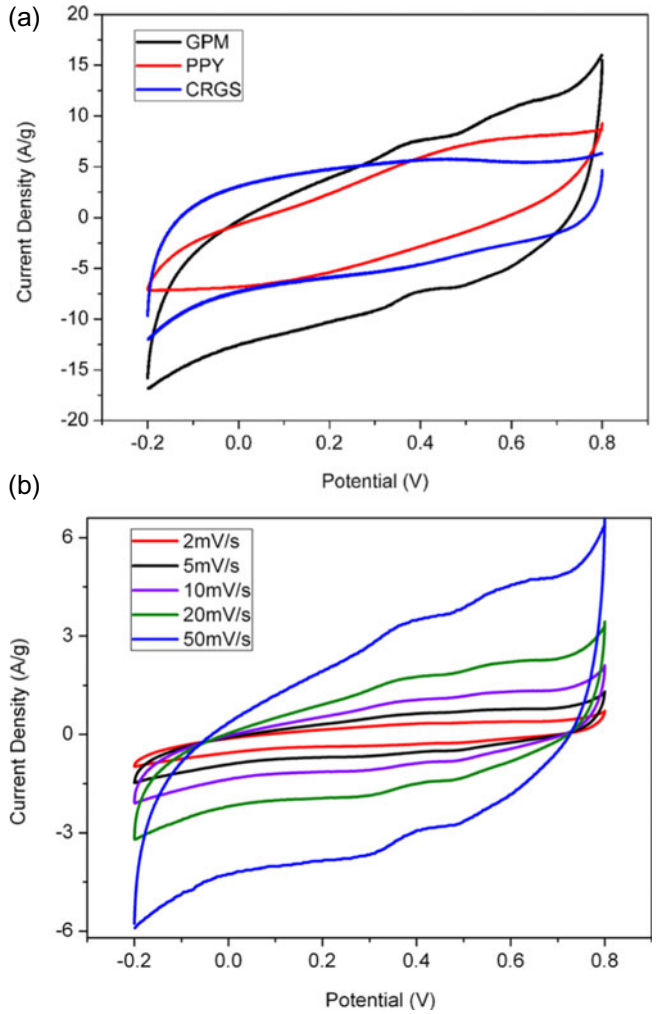

Fig. 4. (Color online) CV curves of GPM, PPY and CRGS: (a) CV curves of PPY, CRGS, GPM at 100 mV s^{-1} and (b) CV curves of GPM at different sweeping rates.

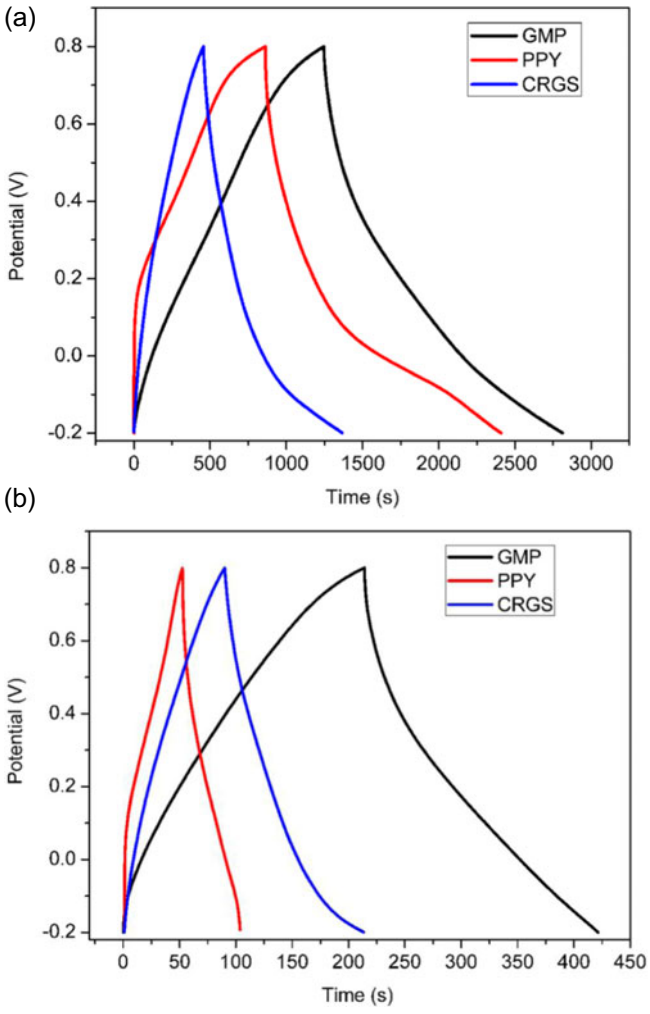

Fig. 5. (Color online) Charge/discharge curves of PPY, CRGS and GPM: (a) charge/discharge curves of PPY, CRGS, GPM at a current density of 0.3 Ag^{-1} and (b) charge/discharge curves of PPY, CRGS and GPM at a current density of 1.5 Ag^{-1}.

test point. It confirms the existence of MnO_2 in GPM. In Figure 2e, the EDS analysis result proves the existence of element N on the test point, verifying the presence of PPY in GPM.

As shown in Figure 3, the Raman spectra provide a clear illustration of the microstructure of the materials. The Raman spectrum of CRGS demonstrates two prominent peaks at 1358 and 1586 cm^{-1}, in accordance with the well-documented data of D and G bands of graphene, respectively [55]. In the spectrum of PPY, the peaks located at 1382 and 1563 cm^{-1} arise from the ring stretching and π-conjugated structure stretching of PPY backbone, respectively [56]. The small peak located at 1048 cm^{-1} corresponds to the C-H in-plane deformation. The two peaks located at 981 and 906 cm^{-1} belong to the ring deformation associated with dication (bipolar) and radical cation (polaron), respectively [55,57]. The spectrum of GPM shows the characteristic bands related to both of its two components, PPY and CRGS. Notably, when compared with CRGS, the band intensity ratio of G to D (I_G/I_D) increases, reflecting the intimate interaction between the π-conjugated PPY and graphene basal plane, without compromising the chemical identity of either PPY or graphene [56]. Different from the graphene-sacrifice mechanism reported by Wei's group [46] which introduces more disorder carbon or defects resulting from the reaction of carbon with $MnO4^-$, in our work, the I_G/I_D increases with the addition of PPY and MnO_2. The fact implies that the graphene contacted with MnO_2 does not have so many defects as the previously reported graphene-MnO_2 by Wei's group [46]. It is expected that the graphene with fewer defects can transfer electron more rapidly and reduce more overall resistance, which consequently improves the rapid capacitance response and electrochemical stability. Furthermore, the spectrum of GPM illustrates a much broader band between 1342 and 1403 cm^{-1}, corresponding to the D band of graphene (1358 cm^{-1}) and the ring stretching of PPY (1382 cm^{-1}). The broadening of the two bands could be explained as follows: with the addition of polar MnO_2, the electrostatic interactions between MnO_2 and PPY as well as MnO_2

https://doi.org/10.1051/epjap/2012120157 Published online by Cambridge University Press

Table 1. Specific capacitances (Fg^{-1}) of composites at different current densities.

Composites	Specific capacitance at current density 0.3 Ag^{-1}	Specific capacitance at current density 1.5 Ag^{-1}	Preserved specific capacitance at current density 1.5 Ag^{-1}
GPM	469.5	312	239
CRGS	259.7	184.9	133
PPY	390.6	77.3	49.5

Table 2. Energy density and power density of materials at different current densities.

Composites	Energy density at current density 0.3 Ag^{-1} (W h/kg)	Energy density at current density 1.5 Ag^{-1} (W h/kg)	Power density at current density 1.5 Ag^{-1} (W/kg)
GPM	65.2	43.3	749
CRGS	36.1	25.7	750
PPY	54.2	10.7	747

and graphene change the electron distribution of PPY and graphene, which makes the electron density variant in different regions of the PPY backbone and graphene basal plane, and consequently broadens the bands. It confirms the intimate interactions between MnO_2 and graphene as well as MnO_2 and PPY.

To exploit the potential application of GPM in supercapacitor, tests were carried out by using CV, galvanostatic charge-discharge and EIS techniques on electrochemical station 660A.

As presented in Figure 4a, the CV curve of CRGS shows ideal rectangular shape when compared with that of PPY nanotube. It indicates that CRGS features good charge propagation within electrode [24]. On the contrary, the CV curve of PPY nanotube is oblique, consistent with the result presented in literature [58]. The CV curve of GPM has the characteristics of both PPY's and CRGS's due to their EDL capacitance and pseudo-capacitance mechanisms, respectively [58,59]. The CV curves of GPM at different sweeping rates were also recorded as shown in Figure 4b. The shapes of GPM's CV curves at high sweeping rates are similar to the curves at low sweeping rates without obvious distortion. The fact that GPM maintains the capacitative response with increasing scanning rates demonstrates its excellent high-rate performance, indicating excellent ionic and electronic transport within the electrode material [56] which can be attributed to the nanotube structures of PPY and MnO_2.

Figure 5 presents the galvanostatic charge/discharge curves at the current densities of 0.3 and 1.5 Ag^{-1}. The specific capacitances of PPY, CRGS and GPM calculated from their charge/discharge curves are listed in Table 1. The calculated energy density and power density of the materials are listed in Table 2. It is evident that the specific capacitance of GPM is higher than that of PPY and CRGS either at different current densities. At a current density of 0.3 Ag^{-1}, the specific capacitance of GPM is 469.5 Fg^{-1}, higher than that of PPY (390.6 Fg^{-1}) and CRGS (259.7 Fg^{-1}). It is also higher than that of the graphene-PPY materials reported in the literature. For example, the capacitance values of graphene-PPY materials are as follows: 409 Fg^{-1} at a scan rate of 10 mV s^{-1} [60], 267 Fg^{-1} at a scan rate of 100 mV s^{-1} [61], 237 Fg^{-1} at a scan rate of 10 mV s^{-1} [59], 318.6 Fg^{-1} at a scan rate of 2 mV s^{-1} [58], 482 Fg^{-1} at a current density of 0.5 Ag^{-1} [43], 285 Fg^{-1} at a current density of 0.5 Ag^{-1} [55], 225 Fg^{-1} at a current density of 0.5 Ag^{-1} [62].

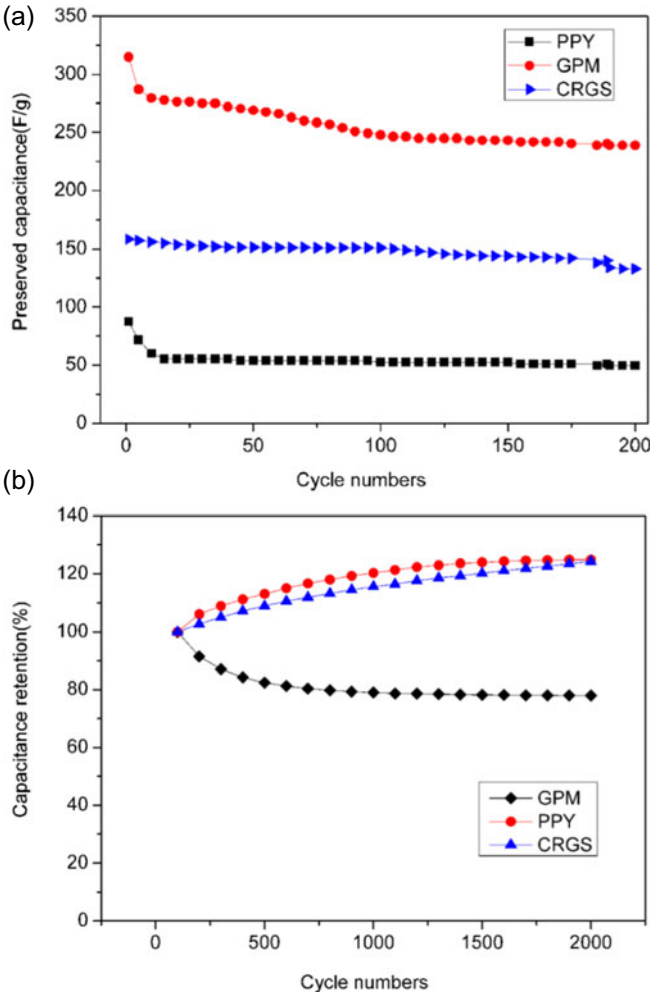

Fig. 6. (Color online) Preserved capacitances of PPY, CRGS and GPM: (a) upon charging/discharging 200 cycles at a current density of 1.5 Ag^{-1} and (b) using CV, upon 2000 cycles at a sweeping rate of 500 mV s^{-1}.

https://doi.org/10.1051/epjap/2012120157 Published online by Cambridge University Press

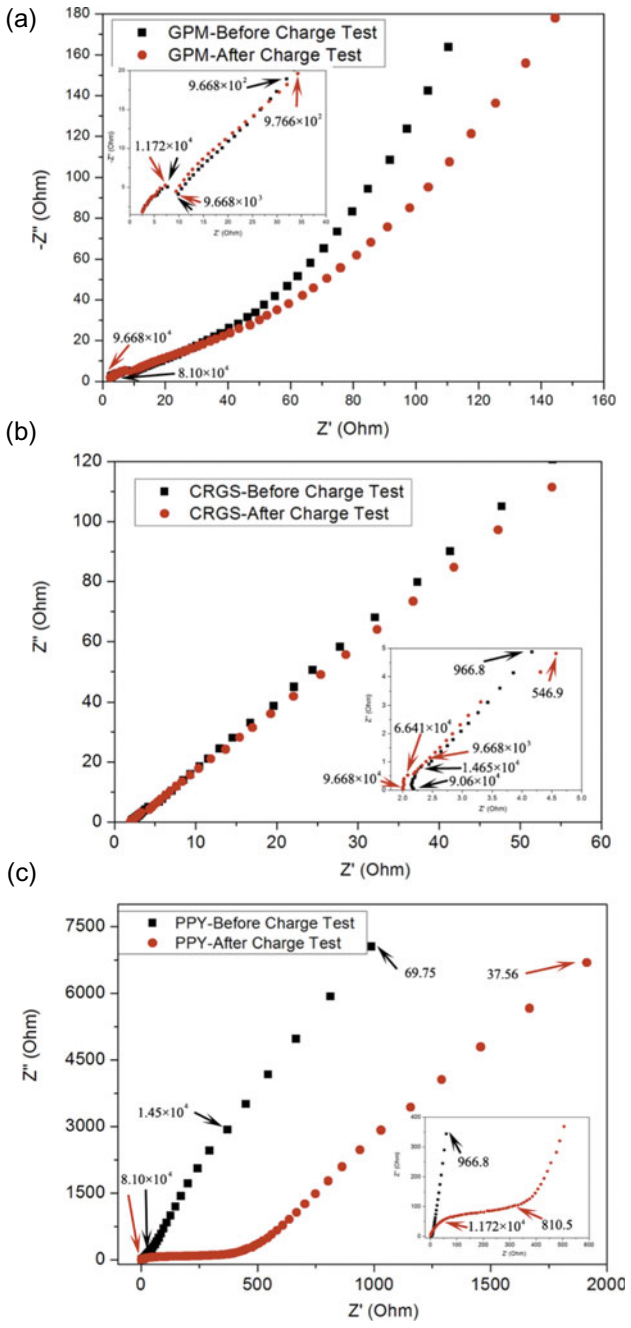

Fig. 7. (Color online) EIS spectra of GPM, PPY and CRGS.

Besides, as presented in Figure 5b, at the current density of 1.5 Ag^{-1}, GPM shows much longer duration than PPY and CRGS. Additionally, the capacitance of GPM (262.5 Ag^{-1}) is also higher than the results reported in the literature. For example, the capacitance of previously reported graphene-PPY composite is 165 Fg^{-1} at a current density of 1 Ag^{-1} [56]. Considering the result at the current density of 0.3 Ag^{-1}, employing nanotube-structures of PPY and MnO_2 together with graphene sheets as supercapacitor electrode material provides a chance to merge the merits of EDL capacitance and pseudo-capacitance mechanisms, which effectively prompts its capacitance performance. It could be interpreted as follows: the nanotube structures of PPY and MnO_2 provide effective electrolyte transport to the active sites of PPY and MnO_2 for enhancing the faradic charge-transfer reactions. Additionally, the existence of high conductive graphene in GPM makes the charges produced by the faradic reactions transport effectively, which prevents the pseudo-capacitive materials' structure conformation from degradation and consequent diminution of the electrical properties with repeated ion exchange [56]. Furthermore, it is in accordance with the structure revealed by SEM and TEM. As illustrated in Figures 1 and 2, the interaction between graphene and MnO_2 is intimate and PPY nanotubes twine graphene and MnO_2 nanotubes together. Therefore, the contact resistances between graphene, PPY and MnO_2 could be effectively reduced, which is highly desirable to improve the electrochemical stability and to achieve rapid charge-discharge characteristics at high discharge current densities [56,63].

To exploit the application of GPM as supercapacitor electrode material at high current density, the preserved specific capacitances of GPM were measured upon 200 charge/discharge cycles at a current density of 1.5 Ag^{-1}, as shown in Figure 6a. After 200-cycle charge/discharge process, the preserved specific capacitance of GPM is 239 Fg^{-1}, higher than that of PPY (49.5 Fg^{-1}) and that of CRGS (133 Fg^{-1}). It implies that the intimately interconnected structure of GPM can comprehensively utilize the advantages of graphene, PPY and MnO_2 at high current density and exhibit a synergic effect.

However, it should be noted that, after 200 charge/discharge cycles at high current density, the preserved capacitance of GPM presents a little attenuation when compared with its initial value (312 Fg^{-1}). Moreover, the preserved capacitance of GPM (239 Fg^{-1}) is only a little higher than that of graphene-PPY composite reported in the literature (165 Fg^{-1}, after long-term charge/discharge cycles at 1 Ag^{-1}) [56]. It may be due to the lack of adhesive addition in electrode material which is immersed in Na_2SO_4 aqueous solution when using three-electrode test system. It leads to the dissolving and breaking up of electrochemically active material at high current density in charge/discharge process. This phenomenon has also been reported previously [24].

To investigate the electrochemical cycling stability of the GPM, using the method reported in the literature [34], we measured the electrochemical stability of GPM by carrying out CV test with the sweeping rate of 500 mV s^{-1} for 2000 cycles. The result illustrates a good stability of GPM because of the existence of graphene and PPY. It can also be seen in Figure 6b. It should be noted that the capacitance of pure MnO_2 is very low because of its poor conductivity. Thus, the capacitance retention of MnO_2 at the sweeping rate of 500 mV s^{-1} cannot be included in Figure 6b.

The EIS analysis was carried out to examine the fundamental behavior of electrode material GPM for supercapacitor application. The impedance spectra of GPM,

https://doi.org/10.1051/epjap/2012120157 Published online by Cambridge University Press

CRGS and PPY were measured in the frequency range of 100 kHz to 0.01 Hz at their open circuit potentials. The initial interfacial charge-transfer resistance (Rc) of CRGS is neglectable and changes little after long-term charge/discharge test. Considering the similarity in its impedance spectra, it demonstrates good electrochemical stability [46]. For PPY, the situation is different. Its initial Rc is low. However, after long-term charge-discharge test at high current density, its Rc increases substantially, which is attributed to the structure change caused by the accumulation of faradic charge. Notably, similar to the situation of CRGS, after long-term charge-discharge test, the impedance spectrum of GPM changes little when compared with the one before test. Furthermore, the Rc of GPM increases little when compared with its initial value. The facts indicate its electrochemical stability. It is due to the presence of good conductive graphene as well as the intimate contact between graphene, PPY and MnO_2, as illustrated in SEM and TEM measurements and Raman analysis (Fig. 7).

4 Conclusions

In summary, through hybridizing CRGS with PPY and MnO_2 nanotube, a novel electrode material GPM was prepared. The morphology and texture characterized by SEM and TEM demonstrate that GPM presents interconnected structure, in which the graphene sheets wrap MnO_2 nanotubes intimately and PPY nanotubes twine graphene and MnO_2 together. The Raman analysis illustrates that the I_G/I_D increases, reflecting the intimate interaction between the π-conjugated PPY and graphene basal plane. When compared with the material reported in the literature, the absence of defects in graphene allows the GPM to transfer electron rapidly, reduces the overall resistance and consequently improves the rapid capacitance response and electrochemical stability. Furthermore, the broadening of the bands confirms the intimate interactions between MnO_2 and graphene as well as MnO_2 and PPY. The CV curve of GPM has the characteristics of both PPY's and CRGS's. The fact that GPM maintains the capacitative response with increasing scanning rates demonstrates its excellent high-rate performance, indicating excellent ionic and electronic transport within the electrode material due to the nanotube structures of PPY and MnO_2. Galvanostatic charge-discharge test demonstrates that the capacitance of GPM is as high as 469.5 Fg^{-1} at the current density of 0.3 Ag^{-1}, higher than that of PPY and CRGS as well as the materials reported in the literature. Moreover, in long-term charge/discharge cycle test at high current density of 1.5 Ag^{-1}, the result confirms that the intimately interconnected structure of GPM can comprehensively utilize the advantages of graphene, PPY and MnO_2 at high current density and exhibit a synergic effect. Additionally, EIS analysis illustrates that the presence of conductive graphene as well as the intimate contact between graphene, PPY and MnO_2 lead the GPM to exhibit good electrochemical stability.

This work has been supported by the National Natural Science Foundation of China (Project No. 51001007).

References

1. K. Zhang et al., Chem. Mater. **22**, 1392 (2010)
2. Q. Wu et al., ACS Nano **4**, 1963 (2010)
3. J.J. Xu et al., ACS Nano **4**, 5019 (2010)
4. D.Y. Liu, J.R. Reynolds, ACS Appl. Mater. Int. **2**, 3586 (2010)
5. X.B. Yan et al., ACS Appl. Mater. Int. **2**, 2521 (2010)
6. H.L. Wang et al., ACS Appl. Mater. Int. **2**, 821 (2010)
7. T. Lu et al., J. Alloys Compd. **509**, 5488 (2011)
8. B. Wang et al., J. Alloys Compd. **509**, 7778 (2011)
9. Z.J. Fan et al., New Carbon Mater. **23**, 149 (2008)
10. Y. Liu et al., Rare Metal Mater. Eng. **37**, 1285 (2008)
11. C.L. Qin et al., Mater. Chem. Phys. **126**, 453 (2011)
12. C.L. Qin et al., Trans. Nonferrous Met. Soc. China **19**, S738 (2009)
13. K.F. Zhou et al., New J. Chem. **34**, 2950 (2010)
14. L. Liu et al., New J. Chem. **35**, 1418 (2011)
15. W.Z. Yang et al., New J. Chem. **35**, 780 (2011)
16. K.F. Zhou et al., New J. Chem. **35**, 353 (2011)
17. C.R. Dean et al., Nat. Nanotechnol. **5**, 722 (2010)
18. D.Y. Chen et al., ACS Appl. Mater. Int. **3**, 3078 (2011)
19. Z. Fan et al., Adv. Mat. **22**, 3723 (2010)
20. X.P. Shen et al., J. Alloys Compd. **506**, 136 (2010)
21. H.F. Xiang et al., J. Alloys Compd. **509**, 7205 (2011)
22. J.R. Miller, R.A. Outlaw, B.C. Holloway, Science **329**, 1637 (2010)
23. Y. Huang, J. Liang, Y. Chen, Small **8**, 1805 (2012)
24. K. Zhang et al., Chem. Mater. **22**, 1392 (2010)
25. S. Liu et al., New J. Chem. **35**, 369 (2011)
26. X. Zhang et al., J. Power Sourc. **173**, 1017 (2007)
27. J.H. Liu et al., Eur. Phys. J. Appl. Phys. **57** (2012)
28. C. Yang, P. Liu, T.M. Wang, ACS Appl. Mater. Int. **3**, 1109 (2011)
29. R. Amade et al., J. Power Sourc. **196**, 5779 (2011)
30. D.P. Dubal et al., J. Alloys Compd. **509**, 8183 (2011)
31. G.A. Snook, P. Kao, A.S. Best, J. Power Sourc. **196**, 1 (2011)
32. T.F. Otero, J. Padilla, J. Electroanal. Chem. **561**, 167 (2004)
33. C. Ye, Z.M. Lin, S.Z. Hui, J. Electrochem. Soc. **152**, A1272 (2005)
34. J. Yan et al., Carbon **48**, 3825 (2010)
35. S. Biswas, L.T. Drzal, Chem. Mater. **22**, 5667 (2010)
36. J.H. Lee et al., Nanotechnology **22**, 29 (2011)
37. Y.W. Ma et al., J. Power Sourc. **196**, 5990 (2011)
38. K.S. Kim, I.J. Kim, S.J. Park, Synth. Met. **160**, 2355 (2010)
39. M. Karahan, Text Res. J. **78**, 718 (2008)
40. A. Malicka-Soczka et al., Acta Phys. Pol. A **115**, 599 (2009)
41. L.Z. Wang et al., in *Proc. of the 2007 Int. Conf. on Advanced Fibers and Polymer Materials*, vols. 1 and 2 (Donghua University, 2007), p. 410, `http://www.clolib/item/21285.aspx`
42. Y.C. Zhao et al., Electrochim. Acta **56**, 1967 (2011)
43. D.C. Zhang et al., J. Power Sourc. **196**, 5990 (2011)
44. J. Liu et al., J. Electrochem. Soc. **159**, A828 (2012)

45. Q. Cheng et al., Carbon **49**, 2917 (2011)
46. Z.J. Fan et al., Carbon **48**, 3825 (2010)
47. Z.S. Wu et al., ACS Nano **4**, 5835 (2010)
48. G.X. Wang et al., Electrochim. Acta **55**, 6812 (2010)
49. Y. Cui et al., J. Am. Chem. Soc. **132**, 13978 (2010)
50. Z.P. Li et al., J. Power Sourc. **196**, 8160 (2011)
51. G.Q. Shi et al., ACS Nano **4**, 1963 (2010)
52. V.C. Tung et al., Nat. Nanotechnol. **4**, 25 (2009)
53. Y. Shi et al., Adv. Mater. **19**, 461 (2007)
54. X.M. Yang et al., Macromol. Rapid Comm. **26**, 1736 (2005)
55. A.R. Liu et al., J. Phys. Chem. C **114**, 22783 (2010)
56. L.T. Drzal, S. Biswas, Chem. Mater. **22**, 5667 (2010)
57. Y.C. Liu et al., Thin Solid Films **374**, 85 (2000)
58. C.H. Xu, J. Sun, L. Gao, J. Mater. Chem. **21**, 11253 (2011)
59. A. Davies et al., J. Phys. Chem. C **115**, 17612 (2011)
60. S. Sahoo et al., Synth. Met. **161**, 1713 (2011)
61. S. Bose et al., Nanotechnology **22**, 295202 (2011)
62. Y.Q. Han, B. Ding, X.G. Zhang, J. New Mater. Electrochem. Syst. **13**, 315 (2010)
63. J. Lee et al., AATCC Rev. **8**, 43 (2008)

https://doi.org/10.1051/epjap/2012120157 Published online by Cambridge University Press